ACCEPTED FOR PUBLICATION IN THE ASTROPHYSICAL JOURNAL
Preprint typeset using LaTeX style emulateapj v. 11/10/09

ASSESSMENT OF STELLAR STRATIFICATION IN THREE YOUNG STAR CLUSTERS IN THE LARGE MAGELLANIC CLOUD.

DIMITRIOS A. GOULIERMIS
Max Planck Institute for Astronomy, Königstuhl 17, 69117 Heidelberg, Germany

DOUGAL MACKEY
Institute for Astronomy, University of Edinburgh, Royal Observatory,
Blackford Hill, Edinburgh, EH9 3HJ, UK
Argelander-Institut für Astronomie, Rheinische Friedrich-Wilhelms-Universität Bonn,
Auf dem Hügel 71, 53121 Bonn, Germany

YU XIN AND AND

BOYKE ROCHAU
Max Planck Institute for Astronomy, Königstuhl 17, 69117 Heidelberg, Germany
Accepted for Publication in the Astrophysical Journal

ABSTRACT

We present a comprehensive study of stellar stratification in young star clusters in the Large Magellanic Cloud (LMC). We apply our recently developed *effective radius method* for the assessment of stellar stratification on imaging data obtained with the Advanced Camera for Surveys of three young LMC clusters to characterize the phenomenon and develop a comparative scheme for its assessment in such clusters. The clusters of our sample, NGC 1983, NGC 2002 and NGC 2010, are selected on the basis of their youthfulness, and their variety in appearance, structure, stellar content, and surrounding stellar ambient. Our photometry is complete for magnitudes down to $m_{814} \simeq 23$ mag, allowing the calculation of the structural parameters of the clusters, the estimation of their ages and the determination of their stellar content. Our study shows that each cluster in our sample demonstrates stellar stratification in a quite different manner and at different degree from the others. Specifically, NGC 1983 shows to be *partially* segregated with the effective radius increasing with fainter magnitudes only for the faintest stars of the cluster. Our method on NGC 2002 provides evidence of *strong* stellar stratification for both bright and faint stars; the cluster demonstrates the phenomenon with the highest degree in the sample. Finally, NGC 2010 is *not segregated*, as its bright stellar content is not centrally concentrated, the relation of effective radius to magnitude for stars of intermediate brightness is rather flat, and we find no evidence of stratification for its faintest stars. For the parameterization of the phenomenon of stellar stratification and its quantitative comparison among these clusters, we propose the slope derived from the change in the effective radius over the corresponding magnitude range as indicative parameter of the *degree of stratification* in the clusters. A positive value of this slope indicates mass segregation in the cluster, while a negative or zero value signifies the lack of the phenomenon.

Subject headings: Magellanic Clouds – galaxies: star clusters – globular clusters: individual: NGC 1983, NGC 2002, NGC 2010 – Hertzsprung-Russell diagram – Methods: statistical – stellar dynamics

1. INTRODUCTION

Stellar stratification is a characteristic phenomenon of star clusters, which has been well documented for more than 50 years. It is directly linked to the dynamical evolution of star clusters (Chandrasekhar 1942; Spitzer 1987), and specifically to the central concentration of the massive stars as the cluster relaxes dynamically, a phenomenon known as *mass segregation* (for detailed reviews see Lightman & Shapiro 1978; Meylan & Heggie 1997). This behavior in massive Galactic globular clusters (GGCs) is well understood and the observed mass segregation is explained as a result of their dynamical relaxation in a timescale, $t_{\rm relax}$, much longer than their ages, τ, as derived from stellar evolutionary models. This *dynamical* mass segregation, thus, forces more massive stars to sink inwards to the center of a cluster through weak two-body interactions.

However, segregation of massive stars is observed also in young star clusters, such as the $\sim$ 30 Myr-old cluster NGC 330 in the Small Magellanic Cloud (Sirianni et al. 2002), or even the $\sim$ 1 Myr-old Galactic starburst NGC 3603 (Stolte et al. 2006). Such systems, supposedly not sufficiently old to be dynamically relaxed, cannot be included in the "traditional" picture of dynamical mass segregation as it occurs in GGCs. For these cases the phenomenon has been – rather tentatively – characterized as *primordial* mass segregation, based on the suggestion that this stellar stratification is due to the formation of the stars in, or near, the central part of the clusters rather than being dynamically driven

Mass segregation at early stages of clustered star formation is indeed predicted by theoretical studies, which suggest that the positions of massive stars for rich young clusters of $\tau << t_{\rm relax}$ cannot be the result of dynamical evolution (Bonnell & Davies 1998). Moreover, the appearance of gas in such clusters reduces further the efficiency of any dynamically driven mass segregation. According to theory, mas-

dgoulier@mpia-hd.mpg.de
dmy@roe.ac.uk
yxin@astro.uni-bonn.de
rochau@mpia-hd.mpg.de

sive protostars can be formed *at the central part* of the protocluster through cohesive collisions and dissipative merging of cloudlets, which lead to extensive mass segregation and energy equipartition among them (Murray & Lin 1996), or through accretion from a distributed gaseous component in the cluster, which leads to mass segregation since stars located near the gravitational center of the cluster benefit from the attraction of the full potential and accrete at higher rates than other stars (Bonnell & Bate 2006).

Both of the aforementioned massive star formation mechanisms predict primordial mass segregation through early dynamical processes at the central part of the protocluster. The significant difference of these processes from the subsequent energy equipartition of the stars in the formed cluster is that the latter, and consequently dynamical mass segregation, is independent of the initial cluster conditions, while the former, and therefore primordial mass segregation, is directly connected to these conditions. In order to achieve a complete understanding of the phenomenon of primordial mass segregation, many related studies are focused on clusters at very early stages of their formation, including a variety of types of stellar systems from loose stellar associations and open clusters to compact massive starbursts.

The Magellanic Clouds (MCs), being extremely rich in young star clusters (e.g., Bica & Schmitt 1995; Bica et al. 1999), offer an outstanding sample of intermediate type of stellar systems, specifically compact young star clusters, which are not available in the Galaxy. In such clusters primordial mass segregation can be sufficiently observed from ground-based observations (e.g., Kontizas et al. 1998; Santiago et al. 2001; Kerber et al. 2002; Kumar et al. 2008), and they are also suitable for more detailed studies of this phenomenon from space with the high-resolving efficiency of the *Hubble Space Telescope* (e.g. Fischer et al. 1998; de Grijs et al. 2002; Sirianni et al. 2002; Gouliermis et al. 2004; Kerber & Santiago 2006). Such studies contribute significantly to the debate about the phenomenon of primordial mass segregation and its origin which which is still ongoing (see, e.g., Kissler-Patig et al. 2007). It is interesting to note that while the existence of the phenomenon itself is being questioned (Ascenso et al. 2009), new methods are still being designed for its comprehensive identification and quantification (e.g., Allison et al. 2009a).

In the first part of our study of stellar stratification we developed and tested a new robust diagnostic method aimed at establishing the presence (or not) of this phenomenon in a cluster (Gouliermis et al. 2009, from here on Paper I). This method is based on the calculation of the mean-square radius, the so-called *effective radius*, of the stars in a cluster for different magnitude ranges, and the investigation of the dependence of the effective radii of each stellar species on magnitude as indication of stellar stratification in the cluster.

1.1. *The Effective Radius Method*

Stellar stratification affects the presently observable physical properties of the star cluster, and thus diagnostic tools for the identification of the phenomenon are based on the detection of mass- or brightness-dependent changes of such properties. Previously established methods involve (i) the study of the projected stellar density distribution of stars of different magnitudes; here, the differences in the exponents of the slopes fitted are seen as proof of mass segregation (e.g., Subramaniam et al. 1993), (ii) the radial dependence of the Luminosity or Mass Function (LF, MF) slope; a gradient of this slope outwards from the center of the cluster indicates stratification (e.g., King et al. 1995), and (iii) the variance of the core radius of the cluster as estimated for stars in specific magnitude (or mass) groups; a trend of this variance with brightness (or mass) signifies stratification (e.g., Brandl et al. 1996). While these methods can provide useful information about the segregation in a cluster, all of them are sensitive to model assumptions, since they strongly depend on data fitting for parametrizing stellar stratification; i.e., functional expressions for the surface density profiles, or the MFs and LFs are required for the derivation of their slopes and core radii.

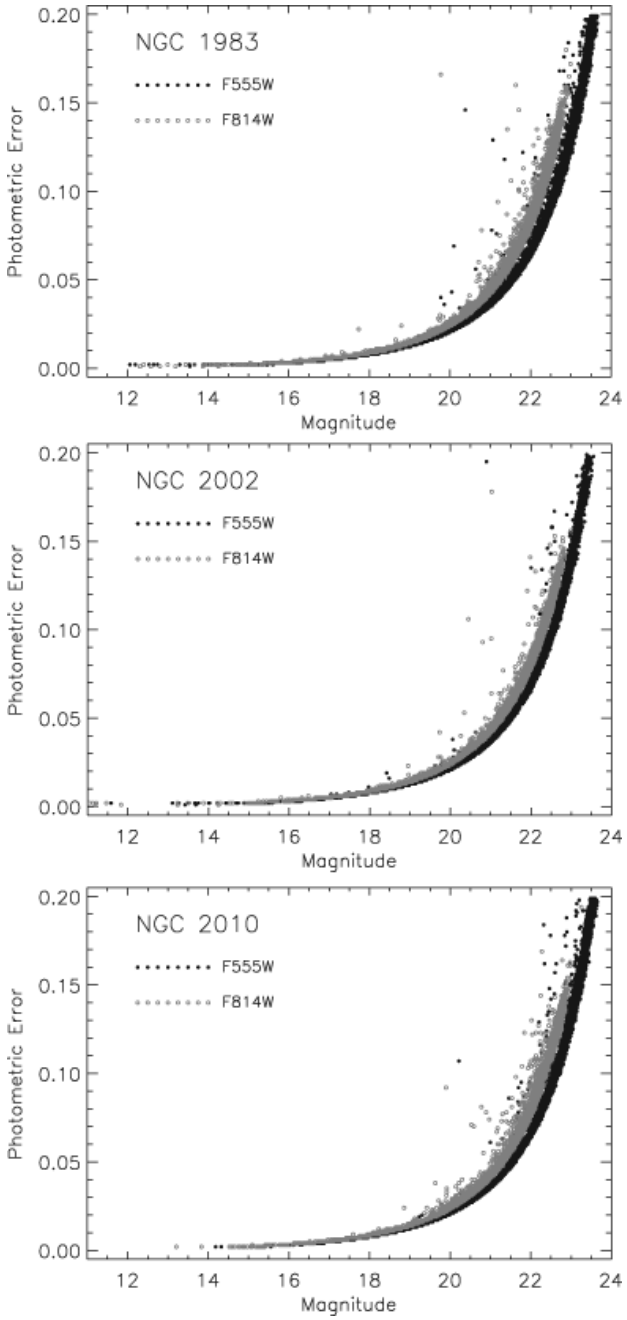

FIG. 1.— Distribution of the uncertainties of our photometry for all stars detected in both the F555W and F814W bands in the areas of the clusters of our sample. Uncertainties in F555W are plotted with filled black and in F814W in open grey circular symbols.

Our method, developed in Paper I for assessment of stellar stratification in star clusters, is based on the notion of the dy-

namically stable *Spitzer radius* of a star cluster, defined as the mean-square distance of the stars from the center of the cluster (e.g., Spitzer 1958). The observable counterpart of this radius, the effective radius, is given by the expression:

$$r_{\rm eff} = \sqrt{\frac{\Sigma_{i=1}^{N} r_i^2}{N}}, \qquad (1)$$

where r_i is the projected radial distance of the ith stellar member of the cluster in a specific brightness range and N the corresponding total number of stars in the same brightness range. Different calculations of the effective radius are performed, each for stars in different brightness ranges that cover the whole observed stellar luminosity function of the cluster. The simple application of this method can yield direct information about the spatial extent (radial distribution) of stellar groups in different magnitude (mass) ranges. In a star cluster, where stratification occurs, the segregated brighter stars are expected to be more centrally concentrated and the corresponding effective radius should be shorter than that of the non-segregated fainter stars. As a consequence, stellar stratification can be observed from the dependence of the effective radius of stars in specific magnitude (mass) ranges on the corresponding mean magnitude (mass). This method is sufficiently described and tested in Paper I, where we show that it performs efficiently in the detection of stellar stratification, provided that the incompleteness of the photometry has been accurately measured and the contamination by the field population has been thoroughly removed. Our diagnosis method is also independent of any model or theoretical prediction, in contrast to those used thus far for the detection of mass segregation.

In this second part of our study of stellar stratification we apply the effective radius method on deep imaging data obtained with the Wide-Field Channel (WFC) of the *Advanced Camera for Surveys* (ACS) onboard the Hubble Space Telescope (HST) of three young star clusters in the Large Magellanic Cloud (LMC) for the investigation of primordial mass segregation in them. Young clusters in the Magellanic Clouds are quite different to each other, so that their study requires the detailed treatment of each cluster individually (see, e.g., §§ 3, 4), and therefore a statistical investigation of the phenomenon of mass segregation in a large sample of such clusters is not yet meaningful. The purpose of the present study is the detailed investigation with the use of a consistent method of individual selected clusters, in order to establish a comprehensive comparative framework for the assessment of mass segregation in young LMC clusters. The objects of interest, clusters NGC 1983, NGC 2002 and NGC 2010, are selected among others also observed with ACS due to their youthfulness and the variety in their characteristics. This selection is made in order to include in this comparative study clusters, which are very different from each other. In § 2 we describe the considered sample of LMC clusters and the corresponding data sets, as well as their reduction and photometry. We study the dynamical status of the clusters and discuss their structural parameters in § 3, and in § 4 we present the observed stellar populations, the decontamination of the stellar samples from the contribution of the local background field of the LMC and the stellar content of the clusters. The application of the diagnostic method is performed for all three clusters in § 5, where we also develop a comparative scheme for the quantification of stellar stratification among different clusters, and we discuss our results. We conclude on them in § 6.

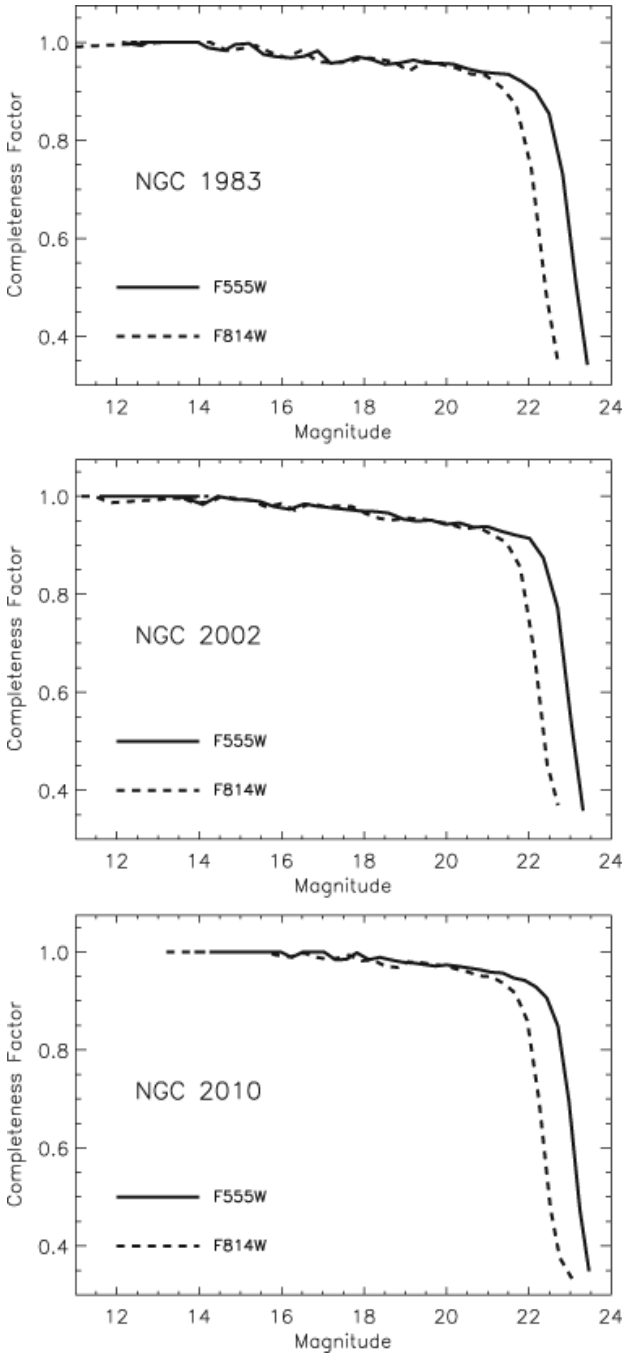

FIG. 2.— Completeness functions for NGC 1983 (top), NGC 2002 (middle), and NGC 2010 (bottom) for both filters F555W (solid line) and F814W (dashed line). Average completeness functions over the whole observed fields of view are shown. It should be noted that completeness is a function of cluster-centric distance, as stars closer to the center of a cluster suffer from high crowding than those farther away.

2. THE STAR CLUSTER SAMPLE

The present study deals with stellar stratification in rich LMC star clusters. Such clusters are known to differ from each other in terms of, e.g., their structural parameters, ages, luminosities and masses (Mackey & Gilmore 2003). Since we focus on the phenomenon of primordial mass segregation we limit our sample to young LMC clusters, and in order to use the most complete available data we select clus-

TABLE 1
ACS/WFC OBSERVATIONS OF THE CLUSTERS OF OUR SAMPLE (HST PROGRAM 9891).

Cluster	R.A. (J2000.0)	DEC (J2000.0)	Filter	Dataset filename	Exposure time (s)	Date
NGC 1983	$05^h27^m44\overset{s}{.}92$	$-68°59'07\overset{''}{.}0$	F555W	j8ne68req	20	October 7, 2003
			F814W	j8ne68riq	20	October 7, 2003
NGC 2002	$05^h30^m20\overset{s}{.}80$	$-66°55'02\overset{''}{.}3$	F555W	j8ne70b5q	20	August 23, 2003
			F814W	j8ne70b7s	20	August 23, 2003
NGC 2010	$05^h30^m34\overset{s}{.}89$	$-70°49'08\overset{''}{.}3$	F555W	j8ne71r5q	20	October 7, 2003
			F814W	j8ne71r9q	20	October 7, 2003

ters observed with ACS/WFC. The advantages introduced to crowded-field photometry of MCs star clusters by the use of ACS, and specifically its Wide-Field Channel, have been documented extensively by studies based on such observations (e.g., Mackey et al. 2006; Rochau et al. 2007; Xin et al. 2008). Consequently, we select three young LMC clusters, NGC 1983, NGC 2002 and NGC 2010, observed with ACS/WFC. These clusters are different from each other, as far as their appearance, structure and stellar content is concerned. Considering that we also wish to investigate the identification and quantification of the phenomenon of stratification in various cluster-hosting environments, we based the selection of these specific clusters on the on the differences between their local surrounding field star populations. We discuss in detail the differences of the clusters themselves in their structure and dynamical behavior in § 3, and in their stellar content in § 4. The decontamination of the true cluster populations from the contribution of the general background field of the LMC, which determines the actual stellar content of the clusters and the stellar sample to be used in our method for assessment of stellar stratification in the clusters is performed in § 4.3.

2.1. *Data Reduction and Photometry*

Our observations come from HST program 9891, a snapshot survey of ~ 50 rich star clusters in the Magellanic Clouds. Imaging was obtained in Cycle 12 using ACS/WFC. As snapshot targets, each cluster was observed for one orbit only, resulting in a single exposure through the F555W filter and another through the F814W filter. Details of the observations for the clusters considered in this paper may be found in Table 1.

The ACS WFC consists of a mosaic of two 4096×2048 pixel CCDs covering an area of approximately $202'' \times 202''$ at a plate scale of 0.05 arcsec per pixel. The two CCDs are separated by a gap roughly 50 pixels wide. The core of each cluster was placed at the center of WFC chip 1. This ensured that the inter-chip gap did not interfere with the main part of the cluster, and meant that each image reached a maximum radius of approximately $\sim 150''$ from the cluster center. A small dither was made between the two exposures of a given target, to help facilitate the removal of cosmic rays and hot pixels; however with only two images per cluster it was not possible to eliminate the gap in spatial coverage due to the inter-chip separation.

The data products produced by the standard STScI reduction pipeline, which we retrieved from the public archive, have had bias and dark-current frames subtracted and are divided by a flat-field image. In addition, known hot-pixels and other defects are masked, and the photometric keywords in the image headers are calculated. We also obtained distortion-corrected (drizzled) images from the archive, produced using the PYRAF task MULTIDRIZZLE.

We used the DOLPHOT photometry software (e.g., Dolphin 2000), specifically the ACS module[1], to photometer the flatfielded (but not drizzled) F555W and F814W images. DOLPHOT performs point-spread function (PSF) fitting using PSFs especially tailored to the ACS camera. Before performing the photometry, we first prepared the images using the DOLPHOT packages ACSMASK and SPLITGROUPS. Respectively, these two packages apply the image defect mask and then split the multi-image STScI FITS files into a single FITS file per chip. We then used the main DOLPHOT routine to simultaneously make photometric measurements on the pre-processed images, relative to the coordinate system of the drizzled F814W image. We chose to fit the sky locally around each detected source (important due to the crowded nature of the targets), and keep only objects with a signal greater than 10 times the standard deviation of the background. The output photometry from DOLPHOT is on the calibrated VEGAMAG scale of Sirianni et al. (2005), and corrected for charge-transfer efficiency (CTE) degradation.

To obtain a clean list of stellar detections with high quality photometry, we applied a filter employing the sharpness and "crowding" parameters calculated by DOLPHOT. The sharpness is a measure of the broadness of a detected object relative to the PSF – for a perfectly-fit star this parameter is zero, while it is negative for an object which is too sharp (perhaps a cosmic-ray) and positive for an object which is too broad (e.g., a background galaxy). The crowding parameter measures how much brighter a detected object would have been measured had nearby objects not been fit simultaneously. We selected only objects with $-0.15 \leq$ sharpness ≤ 0.15 in both frames, and crowding ≤ 0.25 mag in both frames. We also only kept objects classified by DOLPHOT as good stars[2] with formal errors from the PSF fitting less than 0.2 mag in both F555W and F814W. In Figure 1 typical uncertainties in the derived magnitudes of the stars detected in all three clusters are shown for both F555W and F814W filters.

In order to assign a detection completeness fraction to each star, we used DOLPHOT to perform a large number of artificial star tests. For each star in our final cleaned catalogue we first generated a list of 150 associated fake stars using the DOLPHOT utility ACSFAKELIST. We constrained these fake stars to lie close to the real star on the (F555W, F814W) color-magnitude diagram (CMD) – the fake stars were randomly and uniformly distributed in a box of size $2\Delta_V \times 2\Delta_C$ centered on the real star, where Δ_V was the maximum of 0.1 mag

[1] The ACS module of DOLPHOT is an adaptation of the photometry package HSTPHOT (Dolphin 2000). The package can be retrieved from `http://purcell.as.arizona.edu/dolphot/`.

[2] Which have object type 1, as opposed to elongated or extended objects which have object types > 1.

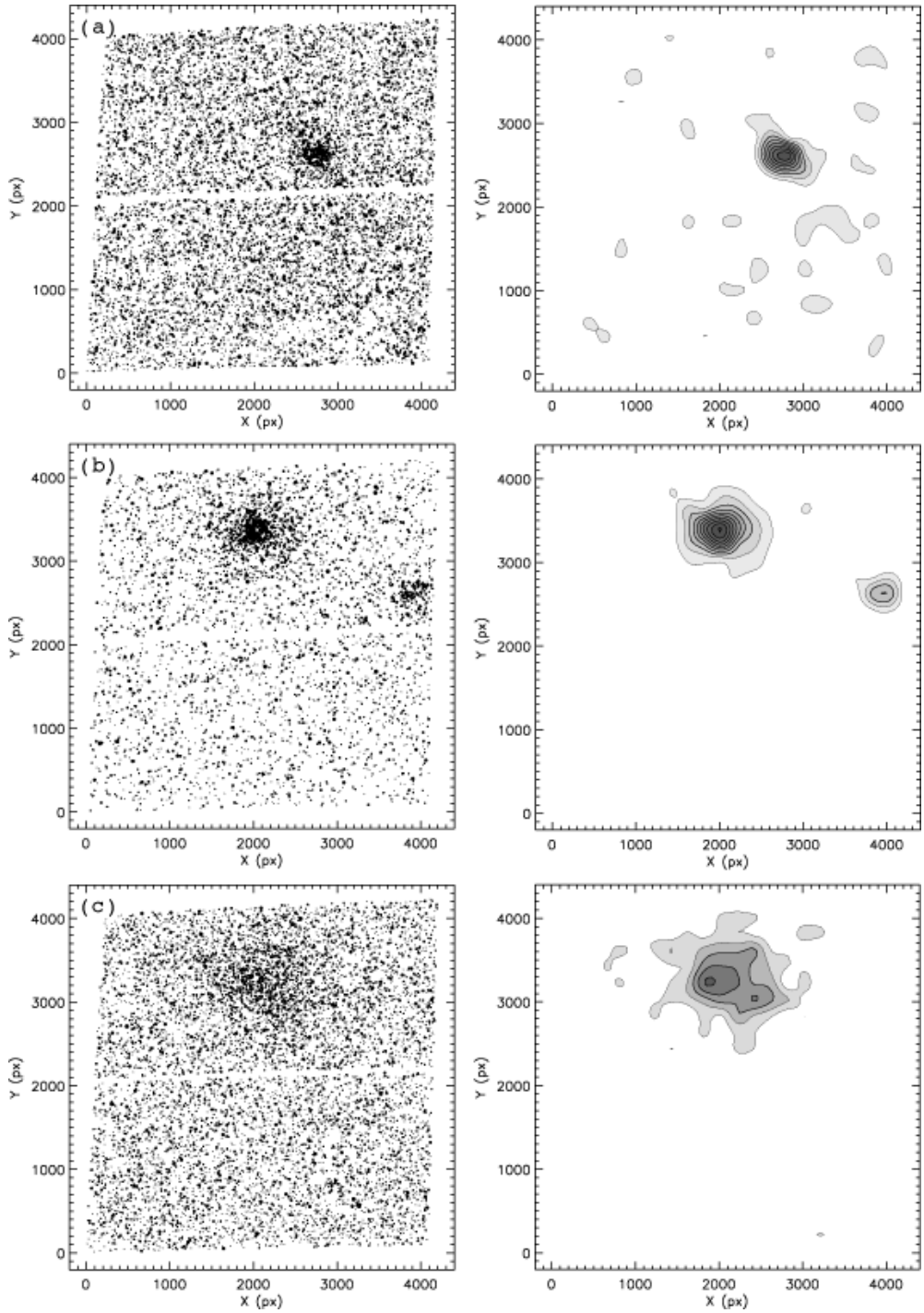

FIG. 3.— The observed ACS/WFC fields-of-view of the clusters (a) NGC 1983, (b) NGC 2002 and (c) NGC 2010 (left panel), with the corresponding stellar density maps constructed with star counts on the photometric catalogs (right panel). Symbol sizes correspond to the brightness of the marked stars. These maps demonstrate that the selected clusters show a variety in size, structure, stellar density and ambient local field (see text in § 3).

and 3 times the uncertainty in the m_{555} magnitude of the real star, and Δ_C was the maximum of 0.1 mag and 3 times the uncertainty in the $(m_{555} - m_{814})$ color of the real star.

We were also careful to constrain the spatial positions of the fake stars. Often this is done so that the fake stars lie at similar cluster-centric radii to the real star under consideration, but with unconstrained position angle. This saves on computation time because the calculations are then valid for groups of real stars at a time, rather than simply on an individual basis. However, because we are dealing with very young clusters in the present work, this implicit assumption of spherical symmetry is not necessarily valid. These objects could potentially still be embedded in gas or dust and thus exhibit a strongly varying background. They are also not very dynamically evolved, so may yet possess azimuthal asymmetries in stellar density as well as numerous randomly placed bright stars. Therefore, we adopted the more computationally expensive method of generating the list of fake stars locally around each real star on the CCD – in this case randomly and uniformly within a radius of $5''$. In doing this we were careful to account for the

TABLE 2
CHARACTERISTICS OF THE CLUSTERS IN OUR SAMPLE DERIVED FROM OUR PHOTOMETRY.

Cluster	Size (pc)	$f_{3\sigma}$ (stars arcsec^{-2})	Age (Myr)	A_V (mag)
NGC 1983	7.3	0.72	28	0.17
NGC 2002	9.4	0.65	18	0.19
NGC 2010	12.5	0.54	159	0.17

NOTE. — Sizes are derived from circular annuli encompassing the 3σ isopleth in the iso-density contour maps of the clusters in the observed regions. Stellar density $f_{3\sigma}$ is measured within these annuli and are given for comparison with the field stellar density of Table 3. Age and interstellar extinction for the clusters are estimated from evolutionary model fitting on the CMDs of stars within the r_c of the clusters. Sizes are given in physical units after a conversion $1' \simeq 15$ pc assuming a distance modulus of $(m-M)_0 \simeq 18.5$ mag (Clementini et al. 2003; Alves 2004; Schaefer 2008) for all clusters.

edges of the chips, including the inter-chip gap.

We then ran DOLPHOT in artificial stars mode on each list of fake stars. When operating in this way DOLPHOT takes the next fake star from the list, adds it to the input images, and then solves for the position and photometric properties of the star using exactly the same parameters as for the original (real star) analysis. Once complete, we took the output photometry and ran it through our quality filters, just as we did for the list of real stars. Finally, we calculated the completeness fraction for a given real star by determining how many of its associated fake stars had been successfully 'found'. We considered a fake star to be found if it was recovered in both F555W and F814W and passed successfully through our quality filter, and provided its output position lay within 2 pixels of its input position. Figure 2 presents the completeness function of our photometry for all considered clusters in both F555W (solid line) and F814W (dashed line) filters.

3. CLUSTER MORPHOLOGIES AND STRUCTURES

3.1. *Morphology of the Clusters*

The stellar charts of the observed ACS/WFC fields of the clusters are shown in Figure 3 (left panel). Our observations show clear differences in the appearance of the three clusters. In order to reveal the spatial distribution of the detected stars and the morphology of the clusters, we performed star counts on our photometric catalogs. The constructed 'iso-density' contour maps for each region are also shown in Figure 3 (right panel). The coordinate system used for these maps is that of the original ACS/WFC pixel coordinates. The star counts were performed in a quadrilateral grid divided in elements with sizes $\sim 190 \times 190$ WFC pix^2 each, which correspond to about $10'' \times 10''$ (or ≈ 2.5 pc $\times$ 2.5 pc at the distance of the LMC). The first isopleth in the contour map indicates the level of 1σ above the mean background density, with σ being the standard deviation of the background density. The subsequent levels are drawn in steps of 1σ. All contours with density equal or higher than the 3σ level, considered as the statistically significant density threshold, are drawn with thick lines. All three star clusters are revealed in these maps as the dominant stellar concentrations in the observed regions. These maps demonstrate that while NGC 1983 is a centrally concentrated compact cluster, NGC 2010 is a quite large and loose cluster, with NGC 2002 being an intermediate case of a large compact concentration. Moreover, NGC 2002 appears to be

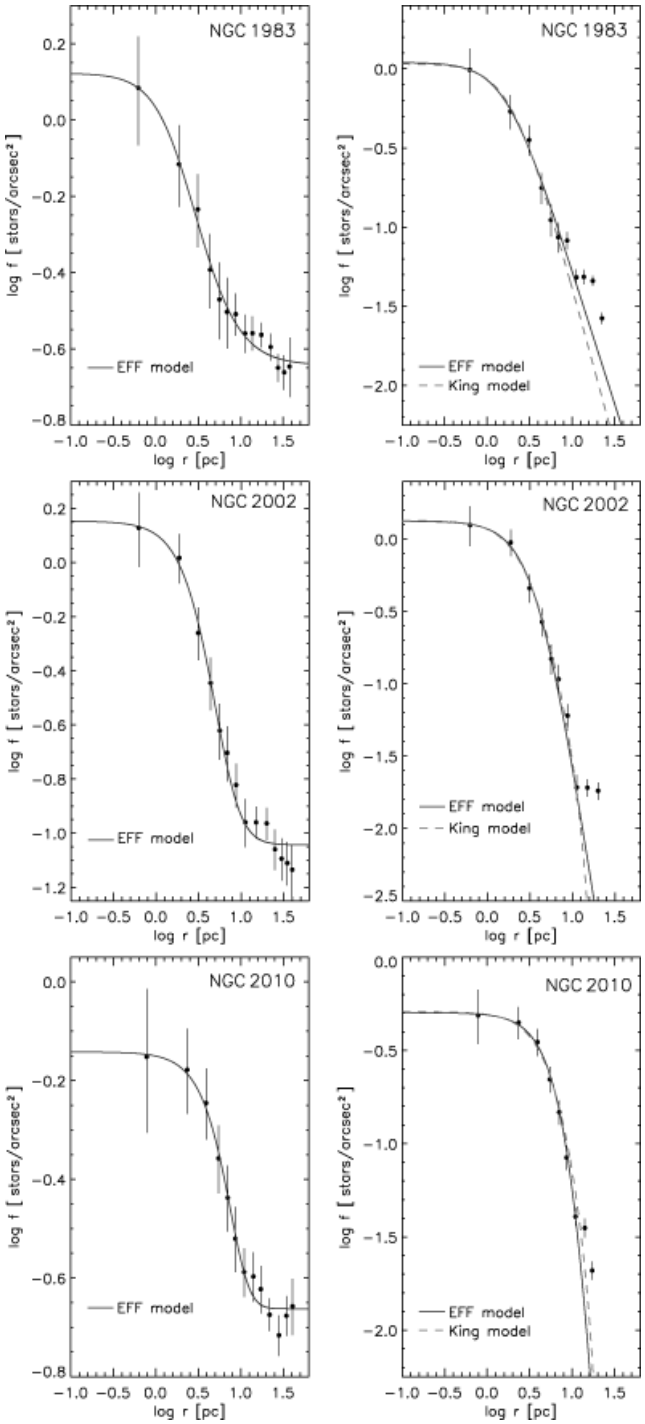

FIG. 4.— Radial surface density profiles of NGC 1983 (top) NGC 2002 (middle), and NGC 2010 (bottom) with the best-fitting King and EFF models superimposed. The error bars represent Poisson statistics. *Left*: Density profiles of all detected stars, including the local field of the LMC. The best-fitting EFF model is over-plotted with a solid blue line. *Right*: Stellar surface density profiles after subtracting the background density level estimated from the best-fitting EFF model shown in the plots on the left. Both EFF and King models are overlaid. Since these clusters are not tidally truncated, the King models are used only tentatively for an estimation of a limiting radius for the clusters. Both models, however, seem to fit very well the density profiles at the inner parts of the clusters deriving comparable core radii. The derived structural parameters based on the best-fitting EFF (solid blue line) and King (dashed green line) models are given in Table 3.

the most spherical cluster in the sample, since NGC 1983 is more elliptical and NGC 2010 is more amorphous, for which,

as indicated by the isopleths of density $\geq 3\sigma$, its most compact part is off-center. The sizes of the clusters as derived from circular annuli considered to encircle the 3σ isopleth for each cluster are given in Table 2. The corresponding surface stellar density of each cluster is also given in this Table.

3.2. *Stellar Surface Density Profiles*

The observed fields cover quite large areas around the clusters in our sample, allowing the construction of the stellar surface density profiles of the clusters at relatively large distances from their centers. We divided the area of each cluster in concentric annuli of increasing steps outwards and we counted the number of stars within each annulus. We corrected the counted stellar numbers for incompleteness according to the corresponding completeness factors on a star-by-star basis. Completeness is a function of both distance from the center of the cluster and magnitude. Let $N_{i,c}$ be the completeness corrected stellar number within the ith annulus. We obtained the stellar surface density, f_i, by normalizing this number to the area of the corresponding annulus as $f_i = N_{i,c}/A_i$, with A_i being the area of the annulus. The observed fields do not always fully cover the complete extent of the clusters, and, therefore, for the truncated annuli, we considered only the available area for the estimation of the corresponding surface density.

The "raw" radial stellar density profiles, meaning the surface stellar density as a function of distance from the center of each cluster, $f(r)$, show a smooth drop outwards away from the centers of the clusters. They drop to a uniform level, which represents the stellar density of the LMC field in the vicinity of the clusters, and it is measured by fitting the models of Elson, Fall & Freeman (1987) to the stellar surface density profiles, $\log f(\log r)$, (Figure 4, left) as described below. In the case of NGC 2002 there is a small increase in the outskirts of the profile due to another neighboring small stellar concentration (see Figure 3). We do not consider this increase in our subsequent analysis on the structure of this cluster. The errors in the profiles reflect the counting uncertainties, representing the Poisson statistics.

3.3. *Structural Parameters*

We applied both the empirical model by King (1962) and the model of Elson, Fall & Freeman (1987) (from here-on EFF) to the stellar surface density profiles of the clusters in order to obtain their structural parameters. The EFF model is suited for clusters which are not tidally limited, while King's empirical model represents tidally truncated clusters. Both models provide the opportunity to derive accurate characteristic radii for the clusters. The core radius (r_c) describes the distance from the center of the cluster where the stellar density drops to the half of its central value and the tidal radius (r_t) is the limit where the stellar density of the cluster drops to zero. The best-fitting EFF and King profiles are found by performing the Levenberg-Marquardt least-squares fit to the considered functions. This fit was performed with IDL[3] (Interactive Data Language) with the use of the specially developed procedure MPFITFUN (Markwardt 2008). For the application of King's model the stellar surface density of the cluster alone (with no contamination from the field) is necessary, while the EFF model does not require any field subtraction. We first apply the latter in order to estimate the core radius and the uniform background level for each cluster. The subtraction of this density level from the measured surface density at each annulus gives the surface density profile of the cluster alone, from which we derive the core and tidal radii.

[3] `http://www.ittvis.com/ProductServices/IDL.aspx`

3.3.1. *Best Fitting EFF Profiles*

From studies of young LMC clusters by EFF it appears that these clusters are not tidally truncated. These authors developed a model more suitable to describe the stellar surface density profile of such clusters:

$$f(r) = f_0(1+r^2/\alpha^2)^{-\gamma/2} + f_{\rm field}, \quad (2)$$

where f_0 is the central stellar surface density, a is a measure of the core radius and γ is the power-law slope which describes the decrease of surface density of the cluster at large radii; $f(r) \propto r^{-\gamma/2}$ for $r \gg a$. The uniform background density level is represented in Eq. (2) by $f_{\rm field}$. The measured parameters α, γ and $f_{\rm field}$, derived from the fitting procedure on our data are given for each cluster in Table 3. According to EFF model, the core radius, r_c, is given from Eq. (2) assuming no contribution from the field as:

$$r_c = \alpha(2^{2/\gamma}-1)^{1/2}. \quad (3)$$

The estimated core radii of the clusters derived from Eq. (3) are also given in Table 3. The best-fitting EFF models are shown superimposed (blue lines) on the stellar surface density profiles of Figure 4.

3.3.2. *Best fitting King Profiles*

In order to construct the density profiles of the clusters alone with no contribution from the field we subtract the background density level, $f_{\rm field}$, from the raw profiles of Figure 4 (left). We then use the field-subtracted profile to derive an indicative tidal radius of the clusters as described by King (1962). According to this model the density profile of a tidally truncated cluster is given as:

$$f(r) \propto \left(\frac{1}{[1+(\frac{r}{r_c})^2]^{\frac{1}{2}}} - \frac{1}{[1+(\frac{r_t}{r_c})^2]^{\frac{1}{2}}}\right)^2, \quad (4)$$

where f is the stellar surface density, r_c and r_t the core and tidal radius, respectively and r is the distance from the center. The tidal radius, which represents the outskirts of the cluster, is found from the formula

$$f(r) = f_1(1/r - 1/r_t)^2, \quad (5)$$

and the core radius, which describes the inner region of the cluster, is given from

$$f(r) = \frac{f_0}{1+(r/r_c)^2}. \quad (6)$$

f_0 describes again the central surface density of the cluster and f_1 is a constant. The best-fitting King profiles apart from core and tidal radii for the clusters, deliver also the concentration parameters, c, defined as the logarithmic ratio of tidal to core radius $c = \log(r_t/r_c)$, which refers to the compactness of the cluster. The derived r_t and c for our clusters are given in Table 3, while r_c derived from the best-fitting King profiles are omitted, as they are found in excellent agreement with those derived above from the EFF profiles. The best-fitting King models of our clusters are shown with green dashed lines superimposed on the radial surface density profiles of Figure 4 (right).

TABLE 3
RESULTS OF THE APPLICATION OF BOTH EFF AND KING MODELS FIT TO THE OBSERVED RADIAL SURFACE DENSITY PROFILES OF THE CLUSTERS IN OUR SAMPLE.

Cluster	EFF Profiles				King Profiles	
	α (pc)	γ	$f_{\rm field}$ (stars arcsec^{-2})	$r_{\rm c}$ (pc)	$r_{\rm t}$ (pc)	c $\log r_{\rm t}/r_{\rm c}$
NGC 1983	1.68 ± 0.28	1.69 ± 0.32	0.23 ± 0.02	1.89 ± 0.43	21.69	0.8
NGC 2002	3.92 ± 0.68	3.91 ± 1.00	0.09 ± 0.01	2.56 ± 0.61	22.33	0.9
NGC 2010	13.32 ± 6.03	9.81 ± 8.04	0.21 ± 0.01	5.19 ± 3.34	28.13	0.7

NOTE. — Parameters α and γ are derived from the best-fitting EFF profile according to Eq. (2). Core radii, $r_{\rm c}$, are derived from the same models with Eq. (3). Tidal radii, $r_{\rm t}$, are measured with Eq. (5) from the best-fitting King models. Concentration parameters, c, are estimated from the measured $r_{\rm t}$ and core radii derived from King models and Eq. (6). All radii are given in physical units after a conversion $1' \simeq 15$ pc assuming a distance modulus of $(m-M)_0 \simeq 18.5$ mag (Clementini et al. 2003; Alves 2004; Schaefer 2008) for all clusters.

In general, both King and EFF models are in good agreement to each other in the inner and intermediate regions of the clusters, which are equally well fitted by both models. However, based on the fact that young compact clusters in the LMC are not tidally truncated, the EFF model should be considered as the best representative for them. On the other hand, the decontamination of the observed stellar samples from the populations of the local LMC field requires the determination of a limiting radius, $R_{\rm lim}$, for the clusters (§ 4.3). Since EFF models do not predict such a radius, we treat the tidal radii derived from the application of King's theory as this radius for each cluster. It should be noted, though, that our clusters are not expected to be dynamically relaxed and therefore, the results on their tidal radii based on the application of King profile fitting should *not* be taken literally but only tentatively for the determination of an indicative *limit* radius for the clusters, and for reasons of comparison. For example, as seen in the charts of Figure 3, NGC 1983 cannot be directly distinguished from the rich stellar field in which it is embedded, as opposed, e.g., to NGC 2002, which shows up as a compact concentration easily separated from its surroundings.

4. STELLAR CONTENT OF THE CLUSTERS

In the stellar charts of the three observed regions, shown in Figure 3 (left), the star clusters immediately appear as the most prominent stellar concentrations. These maps are constructed only from stars detected with photometric uncertainties $\sigma \leq 0.1$ mag in both F555W and F814W filters. In our subsequent analysis we consider only these stars for each observed field. The ACS/WFC field-of-view of NGC 1983 covers 9 641 stars with good photometry, the one of NGC 2002 4 340, and that of NGC 2010 9 006 such stars.

4.1. *Color-Magnitude Diagrams*

The $m_{555}-m_{814}$, m_{814} Color-Magnitude Diagrams (CMDs) of the total observed samples of stars for all three clusters are shown in Figure 5 (top panel). These CMDs of the *Whole Areas* demonstrate the existence of a significant mixture of different stellar populations in each region; from young stars, which cover the main sequence (MS) to the turn-off, belonging to the clusters and their surrounding field, to the evolved Red Giant Branch (RGB) and Red Clump (RC) stars, representing mostly the local background LMC field. The CMDs of Figure 5 indicate that our photometry provides accurate magnitudes for stars with $m_{814} \lesssim 22$ mag. It is interesting to note that as seen from the CMDs of Figure 5 (top), as well as from the stellar charts of Figure 3, the general field of the LMC in the observed regions shows to vary in stellar density. Specifically, both NGC 1983 and NGC 2010 are located in much denser stellar fields than NGC 2002, with the local field of NGC 1983 being particularly rich in red field stars. This is already demonstrated by the measurements of the surface stellar density, $f_{\rm field}$, of the general field of all three clusters in § 3.3 (Table 3; column 4).

The tidal radii, $r_{\rm t}$, of the clusters, as they are derived in § 3.3, basically define the spatial extent of each cluster, and therefore we treat the stars that are located at radial distances from the center of the clusters larger than $r_{\rm t}$ as the best representative stellar populations of the surrounding fields of the clusters. The corresponding CMDs, for which we use the term *Field CMDs*, are shown in Figure 5 (middle panel). In these CMDs the features of both RGB and RC of the general field of the LMC are well apparent in all three observed regions. These populations are well documented as members of the LMC field in various HST studies of the star formation history (SFH) of this galaxy (e.g., Geha et al. 1998; Holtzman et al. 1999; Castro et al. 2001; Smecker-Hane et al. 2002). Specifically, the SFH of the LMC is found to be continuous with almost constant star formation rate (SFR) for over ~ 10 Gyr, with an increase of the SFR at around 1 - 4 Gyr ago (for a summary see Gouliermis et al. 2006, their § 3.1). This old LMC field population is present in all the Field CMDs of Figure 5. Since it covers the same parts in all three of them, we define the age-limits of these stars only on the CMD of the field of NGC 2010. With the use of the Padova grid of evolutionary models (Girardi et al. 2002) for insignificant extinction and metallicity and distance typical for the LMC these limits are found to be $1 \lesssim \tau/{\rm Gyr} \lesssim 10$.

Moreover, the Field CMDs of Figure 5 include also young MS stars, clearly suggesting that the general regions, where all three clusters are located, include young stellar populations that are not members of the clusters. This suggestion does not contradict previous studies on such clusters and their surroundings. Indeed, young compact clusters in the LMC are known to form together in larger structures of young stellar populations, the *Stellar Aggregates* (e.g., Oey et al. 2008), the size of which seems to correlate with the duration of star formation in them (e.g., Efremov & Elmegreen 1999). Such clusters are not isolated as they may be formed in binary or multiple cluster systems (Dieball et al. 2002). An inspection of the general regions where the clusters of our sample are located verifies that none of them is an exception to this general rule. Wide-field images of the regions around the clusters and the whole extent of the LMC in *B*, *R* and *I* were retrieved from the *SuperCOSMOS Sky Survey* (Hambly et al. 2001), available at the *Aladin Sky Atlas* (Bonnarel et al. 2000). These images show that indeed all three clusters are members of larger young structures. Specifically, NGC 1983 is located

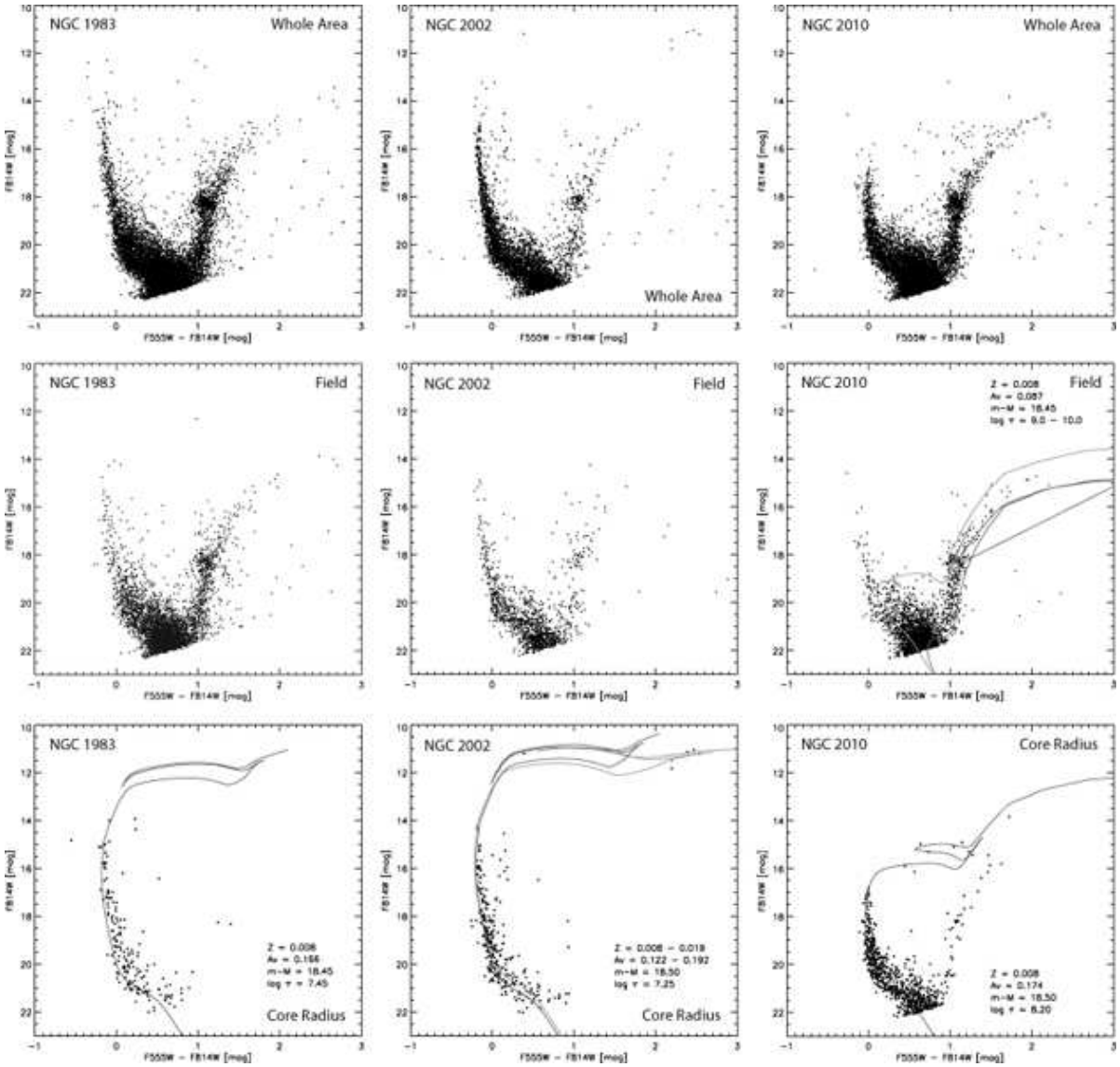

FIG. 5.— The $m_{555}- m_{814}$ vs. m_{814} CMDs of the stars detected with the best photometry (uncertainties $\sigma \leq 0.1$ mag in both filters) in the observed *HST* ACS/WFC areas of the LMC clusters of our sample: NGC 1983 (left), NGC 2002 (middle) and NGC 2010 (right). *Top*: The complete CMDs of all stars detected in the whole observed areas, which demonstrate the mixture of the young stellar populations of the clusters (MS) with those of their surrounding field, and the evolved ones of the general LMC field (RGB, RC). *Middle*: The CMDs of the stars located outside the r_t of the clusters, representing the most probable populations of the local ambient of each cluster. *Bottom*: The CMDs of the stars comprised within the r_c of each cluster, which represent best the true CMDs of the clusters. Isochrones from the grid of evolutionary models by Girardi et al. (2002) are overlaid for an estimate of the age of the clusters and the old field (see § 4.1).

at the central part of the star forming *Shapley Constellation II* (Shapley 1951; McKibben Nail & Shapley 1953) that coincides with the supergiant shell (SGS) *LMC 3* (Meaburn 1980), NGC 2002 belongs to the northern part of *Constellation III* or SGS *LMC 4*, and NGC 2010 is located in one of the eastern nebular filaments of SGS *LMC 9* in *Constellation IX*.

In order to compare these MS field populations with the actual stellar populations of the clusters we select the stars contained in the core radii of the clusters (see § 3.3; Table 3, column 5), as the most probable stellar members, and we construct the corresponding CMDs, which are shown in Figure 5 (bottom panel). A comparison of the Field CMDs with the CMDs of the clusters within their core radii shows that there is a confusion between the young field populations and those of the clusters, especially for NGC 2002 and NGC 1983. The case of NGC 2010 is more straightforward, as it can be seen that while the cluster is somewhat evolved (see discussion below), it seems that it is 'embedded' in a younger field with brighter MS stars. On the other hand, NGC 1983 and NGC 2002 are more complicated cases as both field and clusters seem to comprise the same type of MS stars. Taking into account the similarities of field stars to cluster members in the CMDs, the use of our method for the *statistical* decontamination of the observed stellar samples from the field populations, discussed in § 4.3, becomes quite important. As we show in § 4.4 this method allows us an accurate statistical determination of the most probable stellar members of each cluster.

4.2. *Ages of the Clusters*

We use the CMDs within the core radii of the clusters to derive an estimation of their ages. In the corresponding CMDs of Figure 5 (bottom panel), the best-fitting isochrones from the Padova grid of evolutionary models (Girardi et al. 2002) are also plotted. The process of isochrone fitting of the ob-

served CMD results in an accurate measurement of the age of the system, providing that there are distinguished features in the CMD to be fitted. Moreover, a good estimate of the distance and the interstellar reddening of the cluster is required. For clusters in the LMC, visual extinction is known to vary around very low values (e.g., de Grijs et al. 2002; Gouliermis et al. 2004; Kerber & Santiago 2006), while the distance of the galaxy is also well defined (e.g., Alves 2004; Schaefer 2008). Indeed, for our age estimation we had to vary little both of these parameters around typical values. Since the ACS photometric system is slightly different from the standard Johnson-Cousins system, we estimate the mean extinction in the F555W band, A_{555}, which we arbitrarily symbolize as A_V, using the computations by Da Rio, Gouliermis & Henning (2009). These authors derive a conversion $R_{555} = A_{555}/E(m_{555}-m_{814}) \simeq 2.18$ and $A_{555}/A_{814} \simeq 1.85$ assuming the extinction law of Cardelli et al. (1989) with $R_V \simeq 3.1$. In all cases we assume the typical metallicity of the LMC of $Z \simeq 0.3$ - $0.5\ Z_{\odot}$ (e.g., Westerlund 1997), and therefore we use the models designed for $Z = 0.008$. The derived ages and indicative visual extinction for all three clusters are given in Table 2. Let us consider the results for each cluster individually:

(i) NGC 1983: The CMD of the most prominent member stars of the cluster consists only of the MS, indicating that the cluster is quite young, but making the accurate determination of its age difficult. Indicatively, we apply the youngest isochrone that fits the brighter MS stars with $m_{814} \sim 14$ mag, which shows that the cluster has an age about 28 Myr. The selected isochrone fits best the blue part of the MS for a nominal distance modulus $(m-M)_0 \simeq 18.45$ mag and reddening of $E(m_{555}-m_{814}) \lesssim 0.05$ mag, which corresponds to $A_V \simeq 0.17$ mag.

(ii) NGC 2002: The CMD of NGC 2002 within the r_c of the cluster includes the significant number of five Red Supergiants (RSG) located at $2.2 \lesssim (m_{555}-m_{814}) \lesssim 2.6$ mag and $11 \lesssim m_{814} \lesssim 12$ mag, which helps to constrain accurately the age of the system. However, the isochrone for metallicity $Z = 0.008$ that seems to fit best this cluster with an age of $\tau \simeq 18$ Myr, cannot reach the RSG stars, which thus require the consideration of models of higher metallicity. Indeed the next available models from the Padova grid are those of almost solar metallicity of $Z = 0.019$. The corresponding isochrone for the same age (plotted with a green line in Figure 5) does fit the RSG, implying that either there is a significant change in the metallicity of the cluster, or that the evolutionary models need to be fine-tuned for RSGs in low metallicities. In any case, our data give a fixed age for NGC 2002 of around 18 Myr. It should be noted that while the high metallicity model requires a modest $A_V \simeq 0.12$ mag to fit the CMD, the low metallicity model predicts a higher extinction of $A_V \simeq 0.19$ mag.

(iii) NGC 2010: The CMD of Figure 5 (bottom) for NGC 2010 clearly suggests that this is the oldest cluster in our sample. The existence within r_c of bright stars of $m_{814} \simeq 15$ mag, evolved away from the MS allows us an accurate determination of the cluster age of $\tau \simeq 159$ Myr for $(m-M)_0 \simeq 18.5$ mag and $A_V \simeq 0.17$ mag. However, the appearance in this spatially constrained CMD of a prominent RGB population, clearly suggests that the cluster may comprise a mixture of different stellar populations.

4.3. *Field Decontamination*

As we discuss earlier and seen from the CMDs of Figure 5, all three observed regions suffer from significant contamination by field stars. With no information about cluster-membership probabilities for the observed stars, obtained, e.g., from radial velocities and/or proper motions, the quantitative decontamination of the clusters from the field stars on a statistical basis becomes a fundamental method to obtain the CMD of the complete sample of true stellar members of each cluster. We decontaminate, thus, the observed CMDs from the contribution of the stellar members of the surrounding local field of the LMC with the use of a sophisticated random-subtraction technique.

This field-subtraction algorithm, originally designed by Bonatto & Bica (2007), is already developed in Paper I, where it is also thoroughly described. According to this technique, the successful decontamination of the clusters from the field is based on the definition of the limiting radius, $R_{\rm lim}$, for each cluster. For the clusters in our sample, $R_{\rm lim}$ is given by the tidal radii, r_t, estimated in § 3.3.2 with the use of King's theory. All stars located at distances $r > R_{\rm lim}$ from the center of the cluster are treated as field stars, while the rest (with $r \leq R_{\rm lim}$) are considered as the most probable cluster-member stars. Assuming a homogeneous field-star distribution, the number density of field stars is calculated in the Field CMD (Figure 5; middle) constructed for stars with $r > R_{\rm lim}$, considering also the observational uncertainties in the photometry.

The decontamination process is then applied in three steps for each cluster: (i) Division of the CMDs of the stars with $r \leq R_{\rm lim}$ (cluster region) and of those with $r > R_{\rm lim}$ (offset region), respectively, in 2D cells with the same axes along the m_{814} and $(m_{555}-m_{814})$ directions. (ii) Calculation of the expected number density of field stars in each cell in the CMD of the offset region. (iii) Random subtraction of the expected number of field stars from each cell from the CMD of the cluster region. The algorithm is applied several times using different cell sizes (Δm_{814}, $\Delta(m_{555}-m_{814})$) so that many different decontamination results are derived. From these results we calculate the final probability that a star is identified as a 'true' cluster member, and the final decontaminated CMD of the cluster contains only the stars with the highest probability of being cluster members. This process allows us to minimize any artificial effects intrinsic to the method itself. A detailed description of the mathematical formulation of our method for field-subtraction is given in Paper I.

4.4. *Stellar Populations in the Clusters*

We performed the field-subtraction process, as described above, 15 times for each cluster considering combinations for the CMD cell sizes of $\Delta m_{814} = 0.5$, 1.0, 1.5, 2.5 and 3.0 mag and $\Delta(m_{555}-m_{814}) = 1.0$, 1.5 and 2.0 mag. We obtained, thus, the probability for each star in each sample of being a member of cluster population. Since our method for diagnosis of stellar stratification is completeness-sensitive in the subsequent analysis we limit the sample of stellar members of all three clusters to those detected with our photometry with completeness $\geq 70\%$. The derived stellar samples comprise 424 stars in NGC 1983, 1 102 stars in NGC 2002 and 2 265 stars in NGC 2010 with probability larger than 70% of being true cluster members. Figure 6 shows the corresponding field-star-decontaminated CMDs of the cluster regions for all clusters. Stars found by the field-subtraction method with probability 100% of being cluster members are plotted with thick points. From these CMDs it can be seen that our statistical subtraction of the CMD contamination by the field stars

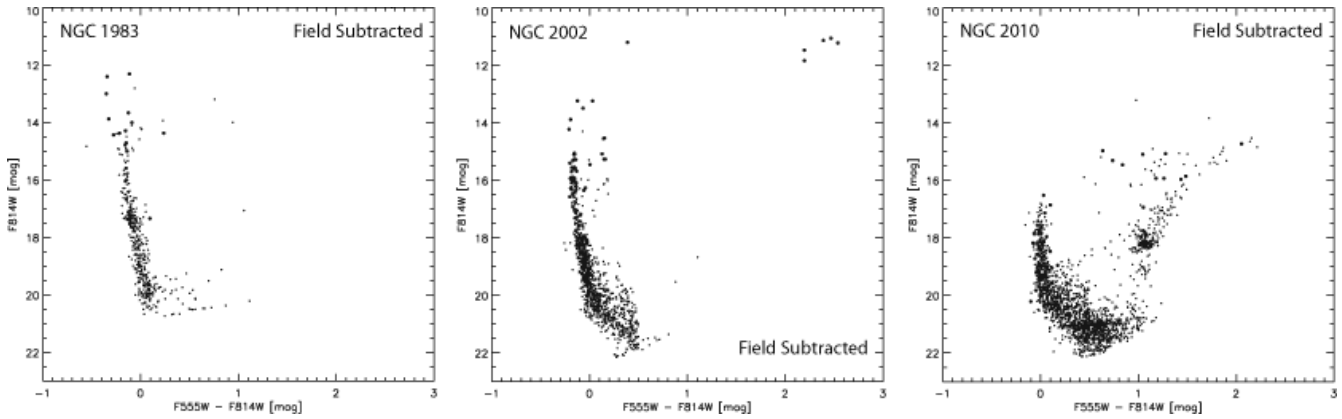

FIG. 6.— The $m_{555}-m_{814}$ vs. m_{814} CMDs of the stars retained as possible members of the clusters after the statistical removal of the contribution of the LMC field from the originally observed CMDs of Figure 5 (top panel). The Field CMDs of the offset regions around the clusters (Figure 5, middle panel) are used as representative of the contaminating populations. Stars with probabilities $> 70\%$ of being true members of the clusters (see § 4.3) are considered for these plots. Stars identified with 100% membership are plotted with thick points.

was efficient in removing both young field populations of the immediate surroundings of the clusters, *and* old populations of the general LMC field. Specifically, for NGC 1983 the MS stars remaining in the CMD of Figure 6, after the application of the field-subtraction, form a sharp narrow MS down to $m_{814} \simeq 21$ mag. This MS resembles that of the CMD within the r_c of the cluster shown in Figure 5 (bottom), with no indication of the broad lower MS stars of the Field CMD of Figure 5 (middle). The CMD of NGC 2002 also demonstrates a very sharp MS similar to the r_c CMD of the cluster. The RSGs located within the r_c of the cluster also remained in the CMD of Figure 6 with 100% of membership probability. As far as NGC 2010 is concerned, the statistical field subtraction removed completely the bright MS young stars identified in § 4.1 as young field stars, while the older MS and evolved stars remained with high probabilities of being true cluster members.

It should be noted that the lower main sequence of the CMDs of the clusters may be also sensitive to any potential pre-main sequence (PMS) population that might exist in such young clusters. However, due to observational constrains, we would be able to detect only the turn-on of these PMS stars, which is known to coincide with the MSTO (see, e.g., Nota et al. 2006; Gouliermis et al. 2007), very close to our detection limit. As a consequence, any PMS population in the clusters would be seriously affected by the incompleteness in our photometry and therefore does not have any significance in the measured stellar numbers. Another bias that may affect the final numbers of low main sequence cluster-members is differential reddening that could displace stars to the red-faint part of the CMD. However, differential reddening in young LMC clusters is known to account for no more than $\Delta E(B-V) \simeq 0.1$ (e.g., Dirsch et al. 2000; Baume et al. 2007), which is well covered by the color uncertainties in our photometry at the low main sequence. As a consequence, differential reddening is not considered in our treatment for field subtraction. It is interesting to note that while the Cluster CMDs of Figure 6 for both NGC 2002 and NGC 2010 show the same features with the corresponding r_c CMDs of the clusters (Figure 5, bottom), that of NGC 1983 shows clear indications of multiple young populations with $m_{814} \lesssim 15$ mag. Indeed, as we discuss in § 4.1, multiplicity is a typical characteristic of young LMC clusters, and naturally it may lead to a merging process and mixing of different stellar populations within one cluster (see e.g., Portegies Zwart & Rusli 2007). As we cannot verify or reject this scenario for NGC 1983, we treat all 424 stars that meet our membership criteria as true members of the cluster. Our diagnostic method for stellar stratification is applied in the following section on the final catalogs of stellar members of the clusters, with 70% membership, the CMDs of which are shown in Figure 6.

5. DIAGNOSIS OF STELLAR STRATIFICATION IN THE CLUSTERS

The *effective radius* method for the diagnosis of stellar stratification is based on the assumption that the observable counterpart of the *Spitzer radius*, the *effective radius*, of stars in a specific magnitude (or mass) range will be a unique function of this range if the system is segregated. In Paper I the comparison of the results of this method with those from the 'classical' methods of the radial dependence of the clusters LFs and MFs, showed that the *effective radius* method behaves more efficiently in the detection of the phenomenon, providing direct proof of stellar stratification in star clusters without considering any model or theoretical prediction, and with no application of any functional fit. In this section we apply this method for the detection and quantification of stellar stratification to the young LMC clusters of our sample.

5.1. *Effective Radii of the Star Clusters*

We calculated the effective radii, $r_{\rm eff}$, of the stars in different magnitude ranges, according to Eq. (1), using the completeness corrected numbers of stars for all three clusters. We performed this calculation only for the star-members of the clusters, as they are established in § 4.4 (CMDs of Figure 6), and we used their brightness measured in the F814W filter, since this filter provided the most complete and accurate photometry (see § 2.1). In order to identify any functional relation between $r_{\rm eff}$ and the corresponding brightness range, we binned the stars according to their magnitudes. Since the measurement of $r_{\rm eff}$ depends strongly to the number of stars per bin, this process naturally inherits systematic uncertainties to the derived relations, because of the fact that some stars could belong to neighboring bins due to photometric uncertainties. Therefore, we performed the same binning process per cluster several times by changing the bin sizes and/or the magnitude limits, within which the stars are binned. We found that a reasonable bin size, which provides good statistics and allows for the detailed observation of the dependence of $r_{\rm eff}$ on magnitude, is that of $0.5 \lesssim \Delta m_{814} \lesssim 1.0$ mag. For this range of bin sizes we did not find any significant change in the general

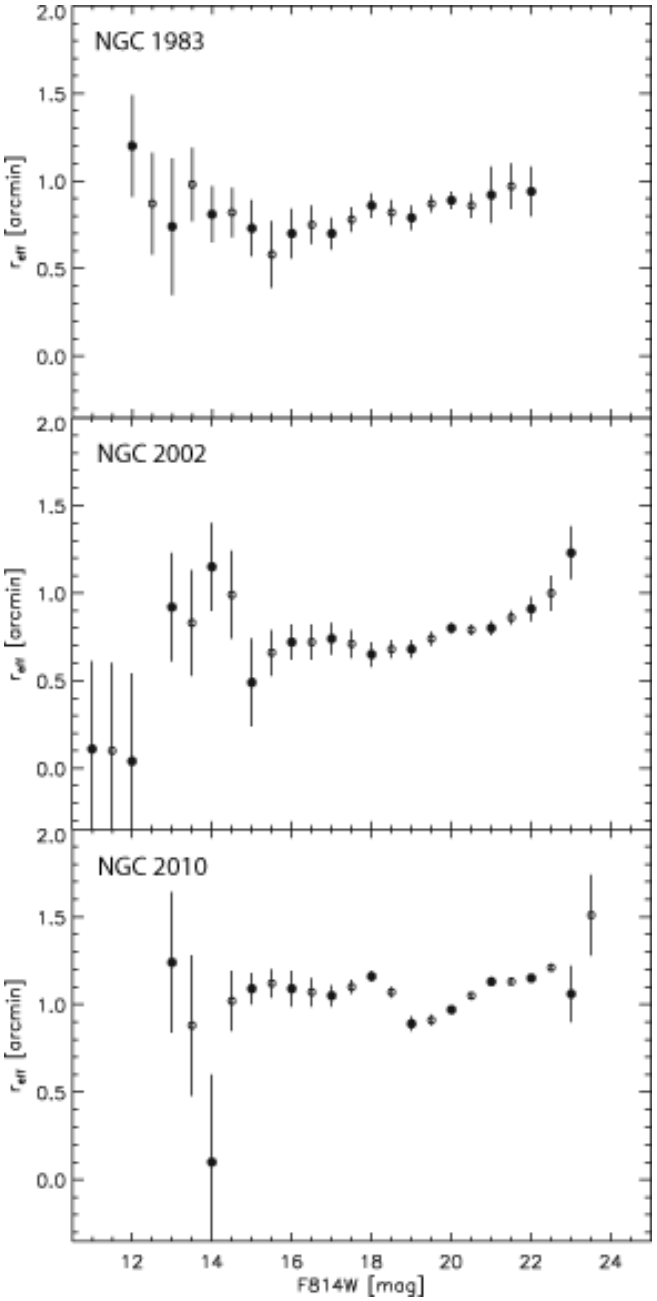

FIG. 7.— Estimated effective radii of stars within different magnitude ranges vs. the corresponding mean magnitude for all three clusters.

trend of $r_{\rm eff}(m_{814})$, which is also found to be independent of the selected magnitude limits for binning the stars.

In Figure 7 we indicatively show the relations between the computed effective radii and the corresponding magnitude bins derived from two different binning processes with bin sizes of 1 mag and magnitude ranges shifted by 0.5 mag from each other. The combination of both distributions with these specific binning characteristics (each plotted with different symbols) provides measurements of $r_{\rm eff}$ for every 0.5 mag range. The derived trends of $r_{\rm eff}(m_{814})$, shown in these plots, are not different from the corresponding distributions derived for $\Delta m_{814} = 0.5$ mag, except of being somewhat smoother. In general the relations of Figure 7 are representative of those found from any applied binning, and therefore we consider them in the following section for the derivation of our results concerning stellar stratification in the clusters.

5.2. *Stellar Stratification in the Star Clusters*

The $r_{\rm eff}(m_{814})$ graphs of Figure 7 are plotted on the same scale for reasons of comparison between the clusters. In these plots it is shown that the effective radius does behave as a function of magnitude, but not necessarily providing proof of stellar stratification for all clusters. A definite indication of stellar stratification would require the effective radii of the faintest stars to be systematically larger than those of the brightest ones for the whole observed brightness range. This is not the behavior we observe at least for two of the three clusters of our sample. Indeed, as we discuss in Paper I, $r_{\rm eff}$ is not a monotonic function of brightness, and mass segregation, *if any*, is not expected to behave in the same manner in every cluster, but rather to depend on the intrinsic stellar characteristics of each of them. For example, while in NGC 2002 there is a trend of fainter stars having systematically larger effective radii for the whole luminosity range, this is not the case for NGC 1983 that shows this trend for only a limited magnitude range, and certainly not for NGC 2010, which one may argue is not even segregated.

Specifically, for NGC 1983, the brightest magnitude bins, down to $m_{814} \simeq 16$ mag, seem to include stars that are located away from the central part of the cluster. Indeed, the brightest stars in the Cluster CMD (Figure 6) with $m_{814} \lesssim 15.5$ mag are found to be distributed within the largest $r_{\rm eff}$ of about $1\farcm2$ away from the center of the cluster and not closer than about $0\farcm6$. On the other hand, taking into account the remaining magnitude bins of $m_{814} \geq 15.5$ mag, the graph of $r_{\rm eff}(m_{814})$ for NGC 1983 provides clear indications that the cluster is segregated with an almost monotonic dependency of larger $r_{\rm eff}$ to fainter stars.

The graph for NGC 2002 is quite different, giving evidence that the cluster is segregated in the whole extend of observed stellar luminosities. There is, however, a dependency of the appearance of a relation between $r_{\rm eff}$ and brightness on the considered magnitude range. Indeed, while the three brightest magnitude bins, comprising six stars (the five RSG and the brightest MS star), correspond to the smallest effective radii, the next fainter bins, which include six more MS stars, show that these stars are located well away from the center of the cluster. Moreover, from the plot of Figure 7 for the fainter stars, it is almost self-evident that they are segregated as the corresponding relation $r_{\rm eff}(m_{814})$ demonstrates an increase of $r_{\rm eff}$ with brightness.

The behavior of this relation for NGC 2010 is quite different from both the previous cases, as there is no general trend for larger effective radii with fainter magnitudes observable, and thus the cluster behaves as if there is no significant stratification occurring. Specifically, apart from the fact that the three brightest magnitude bins are inconclusive, for more faint stars there is a "plateau" in the function $r_{\rm eff}(m_{814})$, which appears rather flat for magnitudes down to $m_{814} \simeq 19$ mag, while for even fainter stars, down to the faintest observed magnitude, the dependence of $r_{\rm eff}$ over m_{814} appears again, giving evidence of mild mass segregation for the faintest stars at the outskirts of the cluster.

5.3. *Degree of Stellar Stratification*

In order to parametrize the phenomenon of stellar stratification as it exhibits (or not) itself in the considered clusters, we assume as null hypothesis that all clusters are segregated,

TABLE 4
MAGNITUDE LIMITS, THE CORRESPONDING EFFECTIVE RADII LIMITS, AND THE DERIVED SLOPES $S_{\rm strat}$ INDICATIVE OF THE DEGREE OF STRATIFICATION FOR SELECTED BRIGHTNESS RANGES FOR ALL THREE CLUSTERS OF OUR SAMPLE.

Cluster	m_{814} (mag)	Δm_{814} (mag)	$r_{\rm eff}$ (arcmin)	$\Delta r_{\rm eff}$ (arcmin)	$S_{\rm strat}$ (mag/arcmin)
NGC 1983	12.0 - 15.5	3.5	1.20 - 0.58	–0.62	–0.177
	15.5 - 22.0	6.5	0.58 - 0.94	+0.36	+0.055
	12.0 - 22.0	10.0	1.20 - 0.94	–0.26	–0.026
NGC 2002	11.0 - 14.5	3.5	0.11 - 0.99	+0.88	+0.251
	15.0 - 23.0	8.0	0.49 - 1.23	+0.74	+0.093
	11.0 - 23.0	12.0	0.11 - 1.23	+1.12	+0.093
NGC 2010	13.0 - 14.0	1.0	1.24 - 0.10	–1.14	–1.140
	14.5 - 18.5	4.0	1.02 - 1.07	+0.05	+0.013
	19.0 - 23.5	4.5	0.89 - 1.51	+0.62	+0.138
	13.0 - 23.5	10.5	1.24 - 1.51	+0.27	+0.026

NOTE. — Negative values of $S_{\rm strat}$ or values close to zero indicate non-segregated clusters at least within the specific magnitude limits (see § 5.2). The third row for every cluster refers to the whole observed magnitude range.

but to a different *degree*. This is evident, as discussed above, from the $r_{\rm eff}$ vs. magnitude plots of Figure 7. This *degree of stratification* in each cluster may be, thus, expressed in terms of the brightness range of its stars, and the effective radius within which they are confined. As a consequence, in order to quantify stellar stratification as observed in every cluster, one may use the two primary output parameters of the effective radius method, i.e., the *magnitude range* and the *corresponding effective radii* of segregation. These parameters actually represent the ranges in magnitudes and radial distances that define *the slope* of the observed relation $r_{\rm eff}(m_{814})$. Naturally, for a non-segregated cluster this slope, $S_{\rm strat}$, should be ≤ 0, as it is derived from the graphs of Figure 7. Considering that a steeper positive slope of this relation represents *a higher degree of stratification*, we parametrize stellar stratification in the clusters by measuring $S_{\rm strat} \equiv \Delta r_{\rm eff}/\Delta m_{814}$ and quantify the phenomenon through this *degree*.

As mentioned above, $r_{\rm eff}(m_{814})$ does not represent a systematic relation throughout the whole observed magnitude range in every cluster, but, as seen in Figure 7, it shows differences depending on the selected magnitudes. For every cluster we select one indicative magnitude limit to separate the bright from the faint stars and measure the corresponding degree of stratification. This selection is based on the magnitude bin, where we observe dramatic changes in the relation $r_{\rm eff}(m_{814})$ in each cluster. As a consequence, we select two magnitude ranges, one spanning from the brightest magnitude bin down to the selected limit, and the other starting at this limit until the faintest magnitude bin, and we estimate their corresponding $S_{\rm strat}$ for all three clusters. These magnitude ranges, the corresponding Δm_{814}, and $\Delta r_{\rm eff}$, and the derived $S_{\rm strat}$ are given in Table 4, along with the derived $S_{\rm strat}$ for the whole observed magnitude range for every cluster. The values of $S_{\rm strat}$, given in this table, correspond to the *degree of stratification* for each cluster in every given brightness range.

5.4. *Results and Discussion*

From the $S_{\rm strat}$ measurements of Table 4 one can see that while indeed the bright stars of NGC 1983 are *not segregated*, stars with $m_{814} \gtrsim 15.5$ mag show a definite trend in their relation $r_{\rm eff}(m_{814})$, indicative of stratification with a degree of +0.06. On average, however, the cluster does not appear to demonstrate stellar stratification. We characterize, thus, NGC 1983 as *partially* segregated cluster. On the other hand, NGC 2002 shows a definite trend of larger $r_{\rm eff}$ for fainter stars within both selected magnitude ranges, as well as for the whole extend of observed magnitudes. It is a definite case of stellar stratification with a degree of stratification of +0.09. Finally, NGC 2010 is the most peculiar case, as the results for the few brightest stars are quite inconclusive, and for the fainter stars with $14.5 \lesssim m_{814} \lesssim 18.5$ mag the cluster appears slightly segregated, with a relation $r_{\rm eff}(m_{814})$ that is rather flat. On the other hand, the most prominent trend in this relation appears for even fainter stars with $m_{814} \gtrsim 18.5$ mag and a degree of stratification $S_{\rm strat} \simeq +0.14$. However, if indeed the cluster was segregated for this magnitude range, the observed trend should appear as a continuation of the (non stratified) relation $r_{\rm eff}(m_{814})$ of the brighter stars. More specifically the $r_{\rm eff}$, where the trend starts for $m_{814} \simeq 19$ mag ($\sim 0\farcm9$) is *smaller* than that of the faintest non segregated stars of $m_{814} \simeq 18.5$ mag with $r_{\rm eff} \sim 1\farcm1$. This behavior of the relation $r_{\rm eff}(m_{814})$ corresponds to fluctuations in the spatial distribution of the faint stars around the center of the cluster rather than to true segregation. As a consequence, we characterize NGC 2010 as *not segregated* cluster.

While the aforementioned results on three clusters cannot be used for a statistically complete interpretation of the phenomenon of stellar stratification in young LMC clusters in connection to their individual characteristics, it is worthwhile to search for any dependence of the degree of stratification to the structural and evolutionary parameters we derived for each cluster in our sample. Concerning the structural parameters shown in Table 3, all clusters are found with comparable concentration parameters, and tidal radii, $r_{\rm t}$, that are not far from each other. The most important difference we find in these parameters is the core radius, $r_{\rm c}$, of NGC 2010, the non (or less) segregated cluster, which is at least two times larger than those of the other two clusters. In addition, from the characteristics of Table 2 it is shown that this cluster is the most extended and least dense in the sample. Moreover, the CMD of the cluster (Figure 6) shows indications of multi-age stellar populations, suggesting that NGC 2010 is a cluster with multiple stellar generations. In such clusters a large fraction of the first generation of stars is lost early in the cluster evolution due to its expansion and stripping of its outer layers resulting from early mass loss associated (e.g., D'Ercole et al. 2008). In gen-

eral, the loose appearance of a low-density cluster with large r_c, comes to the support of this speculation. While this cannot be verified with the present data, it would be reasonable to suggest that the lack of stellar stratification in this cluster will make the effect of early mass loss due to stellar evolution less destructive leading to longer lifetimes (Vesperini et al. 2008).

As far as NGC 2002 is concerned, it is interesting to note that this cluster, being the most segregated in the sample, is actually the youngest (Table 2) and located in a region, which appears to correspond to the emptiest general LMC field of the three (Table 3). Naturally, these observations allow us to suggest that detection of stellar stratification may have been benefitted by the loose contaminating stellar field, and that the observed stellar stratification in NGC 2002 may be *primordial in nature* due to the star formation process, or due to very early dynamical evolution. Indeed recent studies show that cool, fractal clusters can dynamically mass segregate on timescales comparable to their crossing-times, far shorter than usually expected (e.g., Allison et al. 2009b). The exact nature, though, of the observed segregation cannot be fully understood without detailed kinematic information about the cluster members, or deeper photometry that will provide the complete IMF of the cluster. Finally, the observed *partial* stellar stratification in NGC 1983 is driven by the fact that the brightest stars of the cluster are distributed in a wide range of distances from the cluster center. In general, the behavior of $r_{\rm eff}$ as function of stellar magnitude cannot be connected to any specific difference of its characteristics from those of the other clusters, apart from the fact that the cluster belongs to the richest region in field populations, and it is a rather elliptical cluster.

6. CONCLUSIONS

We present a coherent comparative investigation of stellar stratification in three young LMC clusters with the application of a robust method for the assessment of this phenomenon on deep HST imaging. In a cluster where stellar stratification occurs, the segregated brighter stars are expected to be more centrally concentrated than the non-segregated fainter stars. Stellar stratification can, thus, be investigated from the dependence of the radial extent of stars in specific magnitude (mass) ranges on the corresponding mean magnitude (mass). According to this notion, in Paper I (Gouliermis et al. 2009) we developed and verified the efficiency of a robust method for the assessment of stellar stratification in star clusters. This method is based on the calculation of the mean-square radius, the *effective radius* $r_{\rm eff}$, of stars in different magnitude ranges, and the investigation of its dependence on magnitude as indication of stellar stratification in the cluster.

In the present study we apply the *effective radius method* for the detection and quantification of stellar stratification in young star clusters in the LMC. We select three clusters observed with the high resolving efficiency of HST/ACS, specifically NGC 1983, NGC 2002 and NGC 2010, on the basis of the differences in their appearance, structure, stellar content, and surrounding stellar field. Our photometry delivered complete stellar catalogs down to $m_{814} \simeq 22$ - 23 mag for all three observed fields (§ 2.1). The stellar surface density maps of the observed regions, constructed from star counts on the photometric catalogs, demonstrate that all three clusters are morphologically quite different from each other. NGC 1983 appears to be a centrally concentrated, rather elliptical compact cluster, NGC 2002 a compact, spherical stellar concentration, and NGC 2010 a large, loose and rather amorphous cluster (§ 3.1).

The application of both EFF (Elson, Fall & Freeman 1987) and King's (King 1962) models on the stellar surface density profiles of the clusters allowed us the measurement of the background stellar field density of the regions, and the estimation of the core radii, r_c, of the clusters. While these clusters do not seem to be tidally truncated, a tidal radius, r_t is estimated, indicative of the limiting radius of each cluster (§ 3). The latter is essential for the successful application of a random field subtraction technique for the decontamination of the stellar samples of the clusters from their surrounding young stellar ambient and the general LMC field (§ 4.3). We derive the ages of the clusters from the stellar populations comprised within the r_c of the clusters and we find ages of $\tau \simeq 28$ Myr, 18 Myr and 159 Myr for NGC 1983, NGC 2002, and NGC 2010 respectively (§ 4.2).

We finally apply the *effective radius method* for assessing stellar stratification in the clusters and for its quantitative study (§ 5). We bin the stars according to their magnitudes in the F814W filter, and we estimate the corresponding effective radii, $r_{\rm eff}$, for every cluster in our sample. We then plot the derived radii versus the corresponding mean magnitude and we investigate the functional relation, $r_{\rm eff}(m_{814})$, between these parameters. With our method it is shown that stellar stratification behaves differently in every cluster. NGC 1983 appears to be *partially segregated*, since its brightest stellar content does not appear to be centrally concentrated, while its fainter stars show a mild dependency of $r_{\rm eff}$ towards lower values for fainter magnitudes. The results on the bright stars of NGC 2010 show evidence of lack of stratification, since the brightest stars are located quite far away from its center. As far as the faint stars are concerned they show a rather flat $r_{\rm eff}(m_{814})$ relation, with no evidence of segregation in this relation for the faintest stars. Consequently, this cluster is characterized as *not segregated*. Finally, NGC 2002 is found to be well segregated for both its brighter and fainter stars. It is a clear case of proof of stellar stratification with the effective radius method.

We propose the *slope* $S_{\rm strat} \equiv \Delta r_{\rm eff}/\Delta m_{814}$, measured for stars in selected magnitude ranges, as well as in the whole magnitude range, as the most appropriate parameter for the quantification of the *degree of stratification*, and we use it to characterize the phenomenon as it is observed in the clusters. From the derived values of $S_{\rm strat}$ (§ 5.3) we find that NGC 2002 is the most strongly segregated cluster in the sample with a degree of stratification $S_{\rm strat} \simeq +0.09$, NGC 1983 is a partially segregated cluster with $S_{\rm strat} \simeq +0.06$ for the faintest stars with $m_{814} \gtrsim 15.5$ mag, and NGC 2010 is not segregated with indicative $S_{\rm strat} \simeq +0.03$ (§ 5.4). Finally, it should be noted that the extension of this study to a larger sample of LMC clusters observed with HST will provide a more complete picture of the phenomenon of stellar stratification. Naturally, the development of such a comparative scheme, which will include star clusters in the whole extent of the evolutionary sequence, requires a comprehensive set of ACS and, in the near future, WFC3 observations.

D. A. G. kindly acknowledges the support of the German Research Foundation (Deutsche Forschungsgemeinschaft, DFG) through grant GO 1659/1-2, and the German Aerospace Center (Deutsche Zentrum für Luft- und Raumfahrt, DLR) through grant 50 OR 0908. Sincere acknowledgements go also to M. Kontizas and E. Kontizas the collabora-

tion with whom originally planted the seed of the idea for the Effective Radius method. Based on observations made with the NASA/ESA *Hubble Space Telescope*, obtained from the data archive at the Space Telescope Science Institute. STScI is operated by the Association of Universities for Research in Astronomy, Inc. under NASA contract NAS 5-26555.

REFERENCES

Allison, R. J., Goodwin, S. P., Parker, R. J., Portegies Zwart, S. F., de Grijs, R., & Kouwenhoven, M. B. N. 2009a, MNRAS, 395, 1449
Allison, R. J., Goodwin, S. P., Parker, R. J., de Grijs, R., Portegies Zwart, S. F., & Kouwenhoven, M. B. N. 2009b, ApJ, 700, L99
Alves, D. R. 2004, New Astronomy Review, 48, 659
Ascenso, J., Alves, J., & Lago, M. T. V. T. 2009, A&A, 495, 147
Baume, G., Carraro, G., Costa, E., Méndez, R. A., & Girardi, L. 2007, MNRAS, 375, 1077
Bica, E. L. D., Schmitt, H. R., Dutra, C. M., & Oliveira, H. L. 1999, AJ, 117, 238
Bica, E. L. D., & Schmitt, H. R. 1995, ApJS, 101, 41
Bonatto, C., & Bica, E. 2007, MNRAS, 377, 1301
Bonnarel, F., et al. 2000, A&AS, 143, 33
Bonnell, I. A., & Davies, M. B. 1998, MNRAS, 295, 691
Bonnell, I. A., & Bate, M. R. 2006, MNRAS, 370, 488
Brandl, B., et al. 1996, ApJ, 466, 254
Cardelli, J. A., Clayton, G. C., & Mathis, J. S. 1989, ApJ, 345, 245
Castro, R., Santiago, B. X., Gilmore, G. F., Beaulieu, S., & Johnson, R. A. 2001, MNRAS, 326, 333
Chandrasekhar, S. 1942, Principles of Stellar Dynamics. Reprint 2005 by Dover Pubs. (New York). ISBN-13 9780486442730
Clementini, G., Gratton, R., Bragaglia, A., Carretta, E., Di Fabrizio, L., & Maio, M. 2003, AJ, 125, 1309
D'Ercole, A., Vesperini, E., D'Antona, F., McMillan, S. L. W., & Recchi, S. 2008, MNRAS, 391, 825
Da Rio, N., Gouliermis, D. A., & Henning, T. 2009, ApJ, 696, 528
de Grijs, R., Gilmore, G. F., Johnson, R. A., & Mackey, A. D. 2002, MNRAS, 331, 245
Dieball, A., Müller, H., & Grebel, E. K. 2002, A&A, 391, 547
Dirsch, B., Richtler, T., Gieren, W. P., & Hilker, M. 2000, A&A, 360, 133
Dolphin, A. E. 2000, PASP, 112, 1383
Efremov, Y. N., & Elmegreen, B. G. 1999, New Views of the Magellanic Clouds, 190, 422
Elson, R. A. W., Fall, S. M., & Freeman, K. C. 1987, ApJ, 323, 54
Fischer, P., Pryor, C., Murray, S., Mateo, M., & Richtler, T. 1998, AJ, 115, 592
Geha, M. C., et al. 1998, AJ, 115, 1045
Girardi, L., Bertelli, G., Bressan, A., Chiosi, C., Groenewegen, M. A. T., Marigo, P., Salasnich, B., & Weiss, A. 2002, A&A, 391, 195
Gouliermis, D., Keller, S. C., Kontizas, M., Kontizas, E., & Bellas-Velidis, I. 2004, A&A, 416, 137
Gouliermis, D. A., de Grijs, R., & Xin, Y. 2009, ApJ, 692, 1678 (Paper I)
Gouliermis, D., Brandner, W., & Henning, T. 2006, ApJ, 641, 838
Hambly, N. C., et al. 2001, MNRAS, 326, 1279
Holtzman, J. A., et al. 1999, AJ, 118, 2262
Kerber, L. O., Santiago, B. X., Castro, R., & Valls-Gabaud, D. 2002, A&A, 390, 121
Kerber, L. O., & Santiago, B. X. 2006, A&A, 452, 155
King, I. R., Sosin, C., & Cool, A. M. 1995, ApJ, 452, L33
King, I. 1962, AJ, 67, 471
Kontizas, M., Hatzidimitriou, D., Bellas-Velidis, I., Gouliermis, D., Kontizas, E., & Cannon, R. D. 1998, A&A, 336, 503
Kumar, B., Sagar, R., & Melnick, J. 2008, MNRAS, 386, 1380
Lightman, A. P., & Shapiro, S. L. 1978, Reviews of Modern Physics, 50, 437
Mackey, A. D., & Gilmore, G. F. 2003, MNRAS, 340, 85
Mackey, A. D., Payne, M. J., & Gilmore, G. F. 2006, MNRAS, 369, 921
Markwardt, C. B. 2008, in Astronomical Data Analysis Software and Systems XVIII, ASP Conference Series, eds. D. Bohlender, P. Dowler & D. Durand (Astronomical Society of the Pacific: San Francisco), in press (arXiv:0902.2850v1)
McKibben Nail, V., & Shapley, H. 1953, Proceedings of the National Academy of Science, 39, 358
Meaburn, J. 1980, MNRAS, 192, 365
Meylan, G., & Heggie, D. C. 1997, A&A Rev., 8, 1
Murray, S. D., & Lin, D. N. C. 1996, ApJ, 467, 728
Nota, A., et al. 2006, ApJ, 640, L29
Gouliermis, D. A., Henning, T., Brandner, W., Dolphin, A. E., Rosa, M., & Brandl, B. 2007, ApJ, 665, L27
Oey, M. S., King, N. L., Parker, J. W., & Lamb, J. B. 2008, IAU Symposium, 246, 65
Portegies Zwart, S. F., & Rusli, S. P. 2007, MNRAS, 374, 931
Rochau, B., Gouliermis, D. A., Brandner, W., Dolphin, A. E., & Henning, T. 2007, ApJ, 664, 322
Santiago, B., Beaulieu, S., Johnson, R., & Gilmore, G. F. 2001, A&A, 369, 74
Schaefer, B. E. 2008, AJ, 135, 112
Shapley, H. 1951, Publ. Michigan Obs., 10, 79
Sirianni, M., Nota, A., De Marchi, G., Leitherer, C., & Clampin, M. 2002, ApJ, 579, 275
Sirianni, M., et al. 2005, PASP, 117, 1049
Smecker-Hane, T. A., Cole, A. A., Gallagher, J. S., III, & Stetson, P. B. 2002, ApJ, 566, 239
Spitzer, L. 1987, Dynamical Evolution of Globular Clusters. Princeton University Press (Princeton, NJ). ISBN-13 9780691084602
Spitzer, L., Jr. 1958, ApJ, 127, 17
Stolte, A., Brandner, W., Brandl, B., & Zinnecker, H. 2006, AJ, 132, 253
Subramaniam, A., Sagar, R., & Bhatt, H. C. 1993, A&A, 273, 100
Kissler-Patig, M., et al. 2007, "12 Questions on Star and Massive Star Cluster Formation", The Messenger, 129, 69
Vesperini, E., McMillan, S., & Portegies Zwart, S. 2008, IAU Symposium, 246, 181
Westerlund, B. E. 1997, The Magellanic Clouds, Cambridge Astrophysics Series, 29
Xin, Y., Deng, L., de Grijs, R., Mackey, A. D., & Han Z. 2008, MNRAS, 384, 410